Experimental study on geometric and elastostatic calibration of industrial robot for milling application

Yier Wu, Alexandr Klimchik, Stéphane Caro, Christelle Boutolleau, Benoit Furet, Anatol Pashkevich

Experimental study on geometric and elastostatic calibration of industrial robot for milling application

Yier Wu, Alexandr Klimchik, Stéphane Caro, Christelle Boutolleau, Benoit Furet, Anatol Pashkevich

Abstract— **The paper is devoted to geometric and elastostatic calibration of industrial robot for milling application. Particular attention is paid to the analysis of the experimental results and enhancement identification routines. In contrast to other works, the identification results have been validated using separate set of measurements that were not used in calibration. The obtained geometric and elastostatic models essentially improve robot positioning accuracy in milling applications.**

I. INTRODUCTION

In machining of large dimensional parts, application of industrial robots looks very attractive since they provide large workspace comparing to conventional CNC-machines. But because of some particularities of robot kinematics, the end-effector positioning errors are accumulated from link to link and affect on the machining accuracy. Besides, in this application, the elastic deflections of the robot transmissions and mechanical components become significant and comparable with the geometric errors. For this reason, to achieve desired accuracy of the machining process, robot control must rely on the accurate manipulator model that is able to compensate both the geometric errors and the elastic deformations under loadings caused by the machining force/torque.

However in practice, most of the manipulator model parameters are unknown, only nominal values of the principal geometric parameters can be extracted from the manufacturer datasheet. On the other hand, the manipulator elastic parameters can be obtained from the calibration experiments only. So, the identification accuracy for both geometric and elastic parameters becomes critically important.

In the literature, the problem of manipulator model calibration has been in the focus of the research community for several decades. Most of the efforts have been made for manipulator geometric calibration, which has been studied from different aspects (modeling and measurement methods, identification algorithms, etc) [1-6]. Currently, more and more attention is paid to the elastostatic calibration, but the majority of the related works focus on the development of simplified stiffness models and the use of conventional identification techniques [7-8].

Another important issue in this area is related to the identification accuracy improvement and reduction of the measurement noise impact. At present, it has not found enough attention in the literature; only limited number of works directly addressed this problem [9, 10]. An attractive way to improve the identification accuracy without increasing the number of calibration experiments is preliminary *optimization of the measurement configurations*. This approach has been considered in several works [11-13], where the authors adapted the idea of optimal plan of experiments (which was originally developed for linear regression models) to robot calibration. In contrast, in this work measurement configurations have been obtained using new industry oriented performance measure [14], which aims at minimizing robot positioning accuracy after compensation. For this reason, the paper deals with experimental study on the geometric and elastostatic calibration of industrial robot for milling application. It presents calibration methodology and relevant experimental results, with their detailed analysis.

II. EXPERIMENTAL SETUP

The manufacturing cell where the examined robot KUKA KR-270 has been installed is presented in Figures 1 and 2. To identify the desired geometric parameters, the manufacturing cell is equipped with some additional measuring devices that provide us with Cartesian coordinates of the references points for each manipulator configuration. So, entire experimental setup includes the following units:

- KUKA KR-270 manipulator (repeatability 60 μm);
- Robot control system KR-C2;
- Special measurement tool with 3 reference points;
- Laser tracker Leica AT-901 (precision of 10 μm);
- Laser tracker reflector (with precision about 1 μm);
- Personal computer, which is used for data logging.

The experimental setup for manipulator geometric calibration is shown in Figure 1.

*Research supported by ANR (Project ANR-2010-SEGI-003-02-COROUSSO), France and FEDER ROBOTEX, France.

Y. Wu, A. Klimchik and A. Pashkevich are with Ecole des Mines de Nantes, France and with Institut de Recherches en Communications et Cybernétique de Nantes (IRCCyN), France (Tel.+33-251858300; fax.+33-251858349; e-mail: yier.wu@mines-nantes.fr, alexandr.klimchik@mines-nantes.fr, anatol.pashkevich@mines-nantes.fr).

S. Caro is with Centre National de la Recherche Scientifique (CNRS), France and with IRCCyN (e-mail: stephane.caro@irccyn.ec-nantes.fr).

C. Boutolleau is with the Groupe Europe Technologies, France (e-mail: c.boutolleau@europetechnologies.com).

B. Furet is with University of Nantes, France and with IRCCyN (e-mail: benoit.furet@univ-nantes.fr)

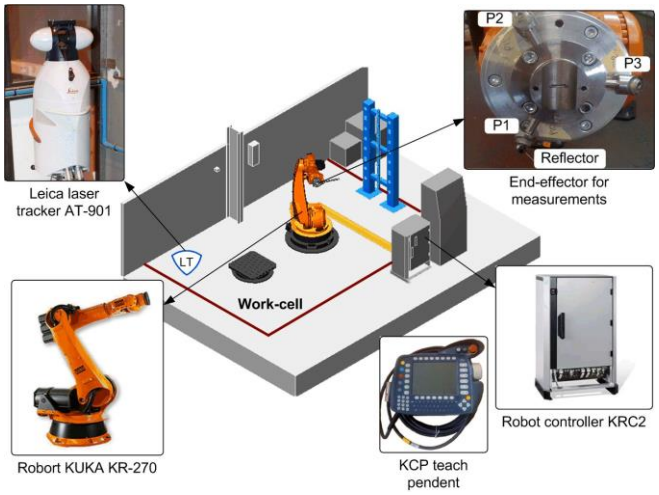

Figure 1. Experimental setup for manipulator geometric calibration

To reduce the influence of the non-geometric factors, the measurements were repeated several times for each configuration, with additional movements of the manipulator end-effector from a current location to its neighborhood and back. As a result of this procedure, the measurement data of each manipulator configuration contain 27 position coordinates (p_x, p_y, p_z for three reference points). The whole data set obtained in experiments contains 432 coordinates p_x, p_y, p_z corresponding to 18 manipulator configurations.

In addition to the experimental devices used in geometric calibration, some extra tools for relevant force application and measurements are used in elastostatic calibration. Corresponding experimental setup is presented in Figure 2. According to the algorithms for the manipulator elastostatic calibration presented in Section III, the experimental procedure is divided into three stages: (i) calibration of the gravity compensator geometry; (ii) calibration of the manipulator elastostatic parameters $k_2, \ldots, k_6$; and (iii) calibration of the manipulator elastostatic parameter k_1.

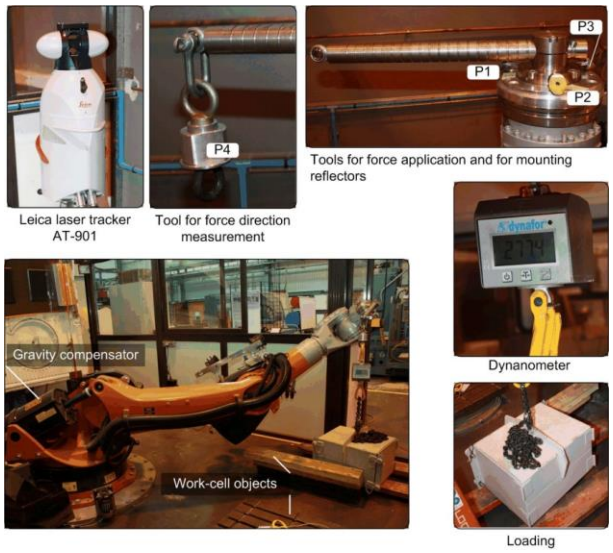

Figure 2. Experimental setup for manipulator elastostatic calibration

III. Mathematical Background

A. Identification of geometric parameters

Let us assume that the measurement tool has n reference points ($n \geq 3$) that are used to estimate relevant vectors of the Cartesian coordinates $\mathbf{p}_i^j = (p_{xi}^j, p_{yi}^j, p_{zi}^j)^T$ for m manipulator configurations $\mathbf{q}_i$. In this notation, the subscript "i" and subscript "j" denote the experiment number and the reference point number, respectively. Correspondingly, the manipulator geometric model can be written as

$$\mathbf{T}_i^j = \mathbf{T}_{base} \cdot \mathbf{T}_{robot}(\mathbf{q}_i, \boldsymbol{\pi}) \; {}^{j}_{tool}; \quad i = \overline{1,m}, \; j = \overline{1,n} \qquad (1)$$

where the vectors $\mathbf{p}_i^j$ are incorporated in the fourth column of $\mathbf{T}_i^j$, the matrix $\mathbf{T}_{base}$ defines the robot base location, the matrices $\mathbf{T}_{tool}^j$, $j = 1,n$ describe the locations of the reference points. Here, the matrix function ${}_{robot}(\mathbf{q}_i, \boldsymbol{\pi})$ describes the manipulator geometry and depends on the actuated coordinates $\mathbf{q}_i$ and the parameters $\boldsymbol{\pi}$ to be estimated. Taking into account that matrix $\mathbf{T}_a^b$ can be split into the rotational $\mathbf{R}_a^b$ and translational $\mathbf{p}_a^b$ components the model (1) can be expressed in the following form

$$\mathbf{p}_i^j = \mathbf{p}_{base} + \mathbf{R}_{base} \cdot \mathbf{p}_{robot}(\mathbf{q}_i, \boldsymbol{\pi}) + \mathbf{R}_{base} \cdot \mathbf{R}_{robot}(\mathbf{q}_i, \boldsymbol{\pi}) \cdot \mathbf{p}_{tool} \qquad (2)$$

This allows us to obtain $3mn$ scalar equations for the calibration purposes, where $n \geq 3$ and m is high enough to ensure identifiability of the desired parameters.

The main difficulty of relevant optimization problem is that some of the unknowns are included in the objective function in highly non-linear way. So, to solve this problem, numerical optimization technique is required. To simplify computations, it is proposed to apply the linearization of geometrical model sequentially and separately with respect to two different subsets of the model parameters (corresponding to the base/tool transformations and the manipulator geometry). Consequently, the identification procedure is split into two steps

Step 1. Assuming that the errors in the base orientation are relatively small, the matrix $\mathbf{R}_{base}$ can be presented as ${}_{base}$ $[\sim \boldsymbol{\varphi}_{base}] + \mathbf{I}$, where $\mathbf{I}$ is a 3×3 identity matrix, vector $\boldsymbol{\varphi}_{base}$ includes the deviations in the base orientation angles, and the operator "$[\sim]$" transforms it into the skew symmetric matrix. Denoting $\mathbf{u}_{tool}^j = \mathbf{R}_{base} \mathbf{p}_{tool}$, equation (2) after several transformations can be rewritten as

$$\mathbf{p}_i^j = \mathbf{p}_{robot}^i \quad \left\lfloor \mathbf{I} \;\middle|\; \left[\sim \mathbf{p}_{robot}^i\right]^T \;\middle|\; \mathbf{R}_{robot}^i \right\rfloor \begin{bmatrix} \mathbf{p}_{base} \\ \boldsymbol{\varphi}_{base} \\ \mathbf{u}_{tool}^j \end{bmatrix} \qquad (3)$$

Applying to the linear system (3) the least-square technique, the desired vectors defining the base and tool transformation parameters can be expressed as follows

$$\left[\mathbf{p}_{base}; \boldsymbol{\varphi}_{base}; \mathbf{u}_{tool}^1; \ldots \; {}^{n}_{tool}\right] \quad \left(\sum_{i=1}^{m} \mathbf{A}_i^{j\,T} \mathbf{A}_i^j \right)^{-1} \left(\; {}_i \quad \mathbf{A}_i^j \; \Delta \mathbf{p}_i \right) \qquad (4)$$

where $\Delta \mathbf{p}_i = (\Delta \mathbf{p}_i^1, \ldots, \Delta \mathbf{p}_i^n)^T$ and

$$\mathbf{A}_i^j = \begin{bmatrix} \mathbf{I} & \left[\sim \mathbf{p}_{robot}^i\right]^T & \mathbf{R}_{robot}^i & \mathbf{0} & \dots & \\ \mathbf{I} & \left[\sim \mathbf{p}_{robot}^i\right]^T & \mathbf{0} & \mathbf{R}_{robot} & \dots & \\ \dots & \dots & \dots & \dots & \dots & \dots \\ \mathbf{I} & \left[\sim \mathbf{p}_{robot}^i\right]^T & \mathbf{0} & & \dots & \mathbf{R}_{robot}^i \end{bmatrix} \quad (5)$$

In this case, the variables defining the location to the reference points are computed as $\mathbf{p}_{tool}^j = \mathbf{R}_{base}^T \cdot \mathbf{u}_{tool}^j$.

Step 2. On the second step, the manipulator geometric parameters $\boldsymbol{\pi}$ are estimated. For this purpose, the principal system is linearized and rewritten in the form

$$\Delta \mathbf{p}^j = \mathbf{J}_{\pi i}^{j(p} \cdot \boldsymbol{\pi} \quad (6)$$

where $\Delta \mathbf{p}_i^j = \mathbf{p}_i - \mathbf{p}_{robot}^i$, the superscript "$(p)$" denotes the positional components, the matrix $\mathbf{J}_{\pi i}^j$ is the identification Jacobian with respect to the reference point j. Applying to this system the least-square technique, the desired vectors of geometric errors $\boldsymbol{\pi}$ can be obtained as

$$\boldsymbol{\pi} \quad \left(\sum_{i=1}^{m} \sum_{j=1}^{n} \mathbf{J}_{\pi i}^{j(p)T} \mathbf{J}_{\pi i}^{j(p)} \right)^{-1} \left(\sum_{i=1}^{m} \sum_{j=1}^{n} \mathbf{J}_{\pi i}^{j(p)T} \Delta \mathbf{p}_i^j \right) \quad (7)$$

It should be noted that, to achieve the desired accuracy, the steps 1 and 2 should be repeated iteratively.

B. Identification of elastostatic parameters

In the frame of enhanced partial pose measurement method [15, 16], each calibration experiment produces a set of vectors $\{\Delta \mathbf{p}_i^j, \mathbf{q}_i, \mathbf{w}_i \mid j = \overline{1,n}\}$. So, the calibration procedure is treated as the best fitting of the experimental data $\left\{\Delta_{\ i}^{\ j}, \mathbf{q}_i, \mathbf{w}_i, i = \overline{1,m}, j = \overline{1,n}\right\}$ by the stiffness model that can be solved using the standard least-square technique. Corresponding system of equations for elastostatic identification that aggregates the desired joint compliances in the vector $\mathbf{k}$ can be presented as

$$\Delta \mathbf{p}_i^j = \mathbf{A}_k^{j(p} (\mathbf{q}_i, \mathbf{w}_i) \cdot \mathbf{k} \qquad i = \overline{1,m},\ j = \overline{1,n} \quad (8)$$

where $\Delta \mathbf{p}_i^j$ is the end-effector deflection for the i-th configuration that is computed for j-th reference point $\mathbf{A}_{k,c}^j = \mathbf{J}_{\theta,c}^j \mathbf{J}_{\theta,c}^{j\ T} \mathbf{w}$.

Applying the least-square technique to the system (8), the estimates of the desired vector of compliances parameters can be computed as

$$\mathbf{k} \quad \left(\sum_{i=1}^{m} \sum_{i=1}^{n} \mathbf{A}_{ki}^{j(p)T} \mathbf{A}_{ki}^{j(p)} \right)^{-1} \cdot \left(\sum_{i=1} \sum_{j=1} \mathbf{A}_{ki}^{j(p)T} \Delta \mathbf{p}_i^j \right) \quad (9)$$

These values can be used to compensate compliance errors caused by external wrench applied to the robot end-effector.

C. Mechanics of gravity compensator

The mechanical structure of the gravity compensator under study is presented in Figure 3. The compensator incorporates a passive spring attached to the first and second links, which creates a closed loop that generates the torque applied to the second joint of the manipulator. This design allows us to limit the stiffness model modification by incorporating in it the compensator torque M_c and adjusting the virtual joint stiffness matrix $\mathbf{K}_\theta$ that here depends on the second joint variable q_2 only.

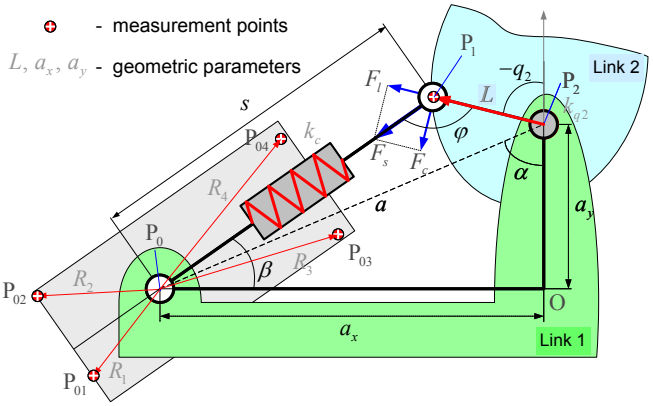

Figure 3. Gravity compensator model

Using the above mentioned property, the equivalent stiffness of the second joint can be expressed as:

$$K_{\theta_2} \quad K_{\theta_2}^0 + K_c\ a\ L\ \eta_{\ 2} \quad (10)$$

where the coefficient η_{q_2} is expressed as follows

$$\eta_{q_2} = \frac{s_0}{s}\left(\frac{a\ L}{s^2} \sin^2(\alpha - q_2) + \cos(\alpha - q_2) \right) - \cos(\alpha - q_2) \quad (11)$$

and depends on the joint variable q_2 and the initial preloading s_0. The definitions of all remaining geometrical parameters is clear from the figure.

Hence, using (10), it is possible to extend the classical VJM-based stiffness model of the serial manipulator by modifying the virtual spring parameters in accordance with the compensator properties. It should be mentioned that the geometrical and elastostatic models of a heavy manipulator with a gravity compensator should include some additional parameters (α, a, L and K_c, s_0 for the presented case) that are usually not included in datasheets. For this reason, the following subsections focus on the identification methodology for the extended set of manipulator parameters.

D. Identification of gravity compensator geometry

In contrast to strictly serial manipulator that can be treated as a principal mechanism of the considered robots, the geometric parameters concerning gravity compensators are usually not included in the technical documentation provided by the robot manufacturers.

According to the proposed stiffness modeling approach, geometrical parameters L, a_x, a affect the equivalent stiffness of the second joint. These geometrical parameters should be identified from the dedicated experimental study. Taking into account particularities of the experimental setup presented in Figure 3, where for each given joint coordinate q_2 the point P_1 is measured, the value of L can be computed as

$$L = \sum_{i=1}^{m} \hat{\mathbf{p}}_i^{\ T} \mathbf{R}\, \hat{\mathbf{u}}_i \Big/ \sum_{i}^{m} \hat{\mathbf{u}}_i^{\ T} \hat{\mathbf{u}}_i \quad (6)$$

where $\hat{\mathbf{p}}_i = \mathbf{p} - m^{-1} \sum_{i=1}^{m} \mathbf{p}_i$ and $\hat{\mathbf{u}}_i = \mathbf{u} - m^{-1} \sum_{i=1}^{m} \mathbf{u}_i$ are centered vectors of the Cartesian coordinates measurements

$\mathbf{p}_i$ and $\mathbf{u}_i = [\cos q_i,\ \sin q_i,\ 0]^T$, m is the number of measurements. Here, the orthogonal matrix $\mathbf{R} = \mathbf{V}\,\mathbf{U}^T$ can be obtained using SVD-factorization $\sum_{i=1}^{m} \hat{\mathbf{u}}_i \hat{\mathbf{p}}_i = \mathbf{U}\,\mathbf{\Sigma}\,\mathbf{V}^T$. The remaining geometrical parameters (a_x and a_y) are *x* and *y* coordinates of the vector

$$\mathbf{p}_0 = \frac{\mathbf{I} - \mathbf{n}\,\mathbf{n}^T}{2}\left(\sum_{j=1}^{k}\sum_{i=1}^{m} \hat{\mathbf{p}}_i^j \hat{\mathbf{p}}_i^{jT}\right)^{-1} \sum_{j=1}^{k}\sum_{i=1}^{m} \hat{s}_i^j \hat{\mathbf{p}}_i^j \quad \frac{\mathbf{n}\,\mathbf{n}}{km} \sum_{j=1}^{k}\sum_{=1}^{m} \hat{\mathbf{p}}_i^j \quad (7)$$

where $\hat{\mathbf{p}}_i^j = \mathbf{p}_i^j - m^{-1}\sum_{l=1}^{m} \mathbf{p}_l^j$, $\hat{s}_i^j = \mathbf{p}_i^{jT}\mathbf{p}_i^j - \ ^{-1}\sum_{l=1}^{m} \mathbf{p}_i^j\ \mathbf{p}_i^j$, $\mathbf{p}_i^j$ is the Cartesian coordinate vector of point P_{0j} for the *i*th measurement, k is the number of reference points and m is the number of measurements. Here, the vector $\mathbf{n}$ is the last column of the matrix $\mathbf{V}$ of the following SVD-factorization $\sum_{j=1}^{k}\sum \hat{\mathbf{p}}_i^j \hat{\mathbf{p}}^{\ T} = \mathbf{U}\,\mathbf{\Sigma}\,\mathbf{V}$.

E. Identification of gravity compensator elasticity

Using the idea of equivalent virtual spring with non-linear stiffness, it is convenient to consider several independent parameters $k_{\theta_{2i}}$ corresponding to each value of q_2. This allows us to obtain linear form of the identification equations that can be easily solved using the standard least-square technique.

Let us denote the set of desired parameters $k_1, (k_{21}, k_{22}\ldots), k_3, \ldots, k_6$ as the vector $\mathbf{k}$, which allows us to present the relevant force-deflection relations in the form $\Delta\mathbf{p} = \mathbf{B}_i^{(p)}\mathbf{k}$, where matrices $\mathbf{B}_i^{(p)}$ are composed of the elements of the observation matrix $\mathbf{A}_{ki}$ that is usually used in stiffness analysis of serial manipulators.

Using these notations, the extended set of elastic parameters that includes all equivalent virtual springs for the second joint can be computed by using the standard least-square technique that leads to

$$\mathbf{k} \quad \left(\sum_{i=1}^{m} \mathbf{B}_i^{(p)^T}\mathbf{B}_i^{(p)}\right)^{-1} \cdot \left(\sum \mathbf{B}_i^{(p)}\ \Delta\mathbf{p}_i\right) \qquad (12)$$

The second step deals with the identification of the gravity compensator parameters and compliance of joint #2

$$K^0_{\ 2} \quad K_c \quad s_0 \cdot K_c\ \Big]^T = \left(\sum_{i=1}^{m_q} \mathbf{C}_i^T \mathbf{C}_i\right)^{-1} \left(\sum_{i=}^{m_q} \mathbf{C}\ \ K_{\theta\ i}\right) \qquad (13)$$

where m_q is the number of different angles q_2,

$$\mathbf{C}_i = \left| 1 \quad -a\,L\cdot\cos\gamma_i \quad a\,L/s\cdot\left(a\,L/s\ \cdot\sin^2\gamma_i + \cos\gamma_i\right)\right| \qquad (14)$$

here $\gamma_i = \alpha - q_{2i}$. Thus, the proposed modification of the previously developed calibration technique allows us to find the manipulator and compensator parameters simultaneously.

IV. Calibration Results

A. Identification manipulator geometry

Using measurement data, the two-step identification procedure has been applied. On the first step, the base and tool transformations have been computed, corresponding results are presented in Tables I and II. On the second step, these transformations have been used for the identification of the manipulator geometric parameters, which are presented in Table III. It should be mentioned that in order to increase the identification accuracy, this two-step procedure has been repeated iteratively (280 iterations, computing time <2 min.).

TABLE I. Identification Results for Base Transformations

	Value, [mm]	CI		Value, [deg]	CI
Laser tracker placement #1					
p_x	-0.023	±0.045	φ_x	-0.004	±0.001
p_y	0.010	±0.032	φ_y	0.001	±0.002
p_z	0.057	±0.044	φ_z	-0.017	±0.001
Laser tracker placement #2					
p_x	-0.099	±0.122	φ_x	-0.009	±0.004
p_y	-0.098	±0.053	φ_y	0.006	±0.004
p_z	-0.076	±0.121	φ_z	-0.013	±0.003

TABLE II. Identification Resuts for Tool Transformations

	RP #1 (P1)		RP #2 (P2)		RP #3 (P3)	
	Value	***CI***	***Value***	***CI***	***Value***	***CI***
p_x, mm	277.23	±0.05	276.49	±0.05	278.44	±0.05
p_y, mm	-46.53	±0.04	-48.25	±0.04	103.73	±0.05
p_z, mm	-93.87	±0.04	94.05	±0.05	-2.17	±0.05

TABLE III. Identification Results for Geometric Parameters

Parameter	p_{x1}	p_{y1}	φ_{x1}	Δq_2	p_{x2}	φ_{x2}
Unit	[mm]	[mm]	[deg]	[deg]	[mm]	[deg]
Value	-0.353	0.426	0.015	-0.007	0.458	0.022
CI	±0.086	±0.272	±0.005	±0.005	±0.082	±0.014
Parameter	φ_{z2}	Δq_3	p_{x3}	p_{z3}	φ_{z3}	Δq_4
Unit	[deg]	[deg]	[mm]	[mm]	[deg]	[deg]
Value	-0.023	-0.023	-0.214	-0.508	-0.011	0.001
CI	±0.005	±0.019	±0.089	±0.363	±0.017	±0.008
Parameter	p_{y4}	p_{z4}	φ_{z4}	Δq_5	p_{z5}	φ_{z5}
Unit	[mm]	[mm]	[deg]	[deg]	[mm]	[deg]
Value	-0.167	-0.018	0.025	-0.011	0.016	-0.008
CI	±0.113	±0.073	±0.015	±0.027	±0.104	±0.018

For the comparison purposes, the manipulator accuracy improvement has been studied based on the residual analysis before and after calibration. Corresponding results are presented in Table IV, which includes the maximum and root mean square (RMS) values of the relevant residuals. As follows from the results, both types of the residuals have been essentially reduced after calibration. In particular, the maximum values have been reduced by a factor of 4 and 3.5, while the RMS values of these two criteria have been decreased by a factor of 5.3 and 5.5, respectively.

TABLE IV. Manipulator Accuracy Improvement After Geometric Calibration Based on Residual Analysis

Type of residuals		**Before calibration**	**After calibration**	**Improvement factor**
Coordinate	***max***	1.25	0.32	4.0
based, [mm]	***RMS***	0.54	0.10	5.3
Distance	***max***	1.31	0.39	3.5
based, [mm]	***RMS***	0.94	0.17	5.5

In order to evaluate the calibration results, the residuals from the identification equations have been computed for each coordinate separately, corresponding histograms are shown in Figure 4. As follows from detailed analysis, the residuals tend to follow the normal distributions with zero mean and parameter σ equal to 0.10 mm, 0.09 mm, and 0.11 mm for X-, Y-, and Z- direction, respectively. The latter

allows us to conclude that the measurement noise parameter σ in experiments is equal to 0.1 mm. This value is higher than the precision of the laser tracker (0.01 mm), the difference can be caused by limitations of the geometric model, which does not take into account the elastostatic deformations due to gravity, the friction/backlash in joints and other factors that influence on the robot repeatability (±0.06 mm). Nevertheless, geometric calibration ensures essential improvement of the robot accuracy.

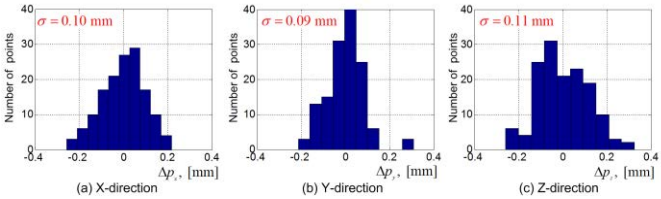

Figure 4. Histograms of residual distribution along X-, Y-, and Z-directions after geometric calibration

B. *Identification compensator geometry*

The principal geometric parameters of the gravity compensator are L, a_x and a_y (see Figure 3). They can be identified using relative locations of points P_0 and P_1 with respect to P_2. Corresponding measurement data for the set of angles $q_2 = \{0°, -30°, -60°, -90°, -120°, -140°\}$ have been processed using two identification algorithms. The first algorithm is aimed at matching the set of points $\{\mathbf{p}_1^i\}$ with additional set of angles $\{q_2^i\}$, that allows us to identify the desired circle radius L. The second algorithm uses sets of point positions $\{\mathbf{p}_{01}^i\},...,\{\mathbf{p}_{04}^i\}$ to determine the relative location of point P_0 with respect to P_2. The identified parameters and confidence intervals are given in Table V.

TABLE V. IDENTIFICATION RESULTS FOR THE COMPENSATOR GEOMETRIC PARAMETERS

	L, [mm]	a_x, [mm]	a_y, [mm]
Value	184.72	685.93	123.30
CI	± 0.06	± 0.70	± 0.69

C. *Identification of elastostatic parameters*

Using the identification results for the gravity compensator geometry, it is possible to evaluate the variation of the equivalent stiffness of the second joint caused by the gravity compensator impact. As follows from dedicated analysis, the compensator impact is highly non-linear, differs throughout the robot workspace and highly depends on the spring preloading s_0. Nevertheless, it is possible to treat the value of k_2 as a constant in the neighborhood of each q_2. This allows us to use the linear system of identification equations. In accordance with the geometric parameters of the gravity compensator and the manipulator joint limits, five values of joint q_2 have been selected (-0.01˚, -25.2˚, -56.9˚, -99.8˚, -140˚). So, the desired vector of the elastostatic parameters $\mathbf{k}$ includes four constant compliance parameters $\{k_3, k_4, k_5, k_6\}$ and a 5×1 vector $\{k_{21},...,k_{25}\}$ that describes the configuration-dependent compliance parameters for different values of joint angle q_2.

In usual engineering practice, it is assumed that all measurements are corrupted by the same measurement noise. However, for the laser tracker used in our experiments, the precision highly depends on the measurement direction and varies throughout the robot workspace. In this case, the covariance matrix can be still assumed to be diagonal, but with non-equal diagonal terms. For comparison purposes, the identification has been performed using both Ordinary Least-Square (OLS) and Weighted Least Square (WLS) techniques. Corresponding values of the elastostatic parameters are presented in Table VI. The results show that the confidence intervals for OLS and WLS have intersections for all parameters of interest. Moreover, the confidence intervals for WLS are always inside confidence intervals for OLS and are considerably smaller. Using the obtained values of $\{k_{21},...,k_{25}\}$, it has been identified an equivalent parameter k_2, which is used in stiffness modeling of the manipulator with the gravity compensator. The identified compensator elastostatic parameters are presented in Table VII, which also includes the compensator compliance and preloading.

The obtained manipulator elastostatic parameters can be used to improve the robot accuracy by compensation of the robot deformations under the external loading. For comparison purposes, the accuracy improvement has been studied based on the residual analysis. Similar to the geometric case, two types of residuals have been examined, the coordinate- and distance-based ones. Corresponding results are presented in Table VIII. As follows from them, maximum and RMS residuals have been essentially reduced after calibration by a factor of 6.0 and 6.5 respectively.

TABLE VI. COMPARISON OF THE ORDINARY AND WEIGHTED LEAST SQUARE TECHNIQUES ([RAD × μM/N])

k_i	OLS	WLS	Mutual location of CI	CI_{OLS}	CI_{WLS}	$\frac{\sigma_{OLS}}{\sigma_{WLS}}$
k_{21}	0.297	0.287		3.4%	0.09%	40.5
k_{22}	0.287	0.277		4.2%	0.13%	33.2
k_{23}	0.315	0.302		5.9%	0.18%	33.9
k_{24}	0.302	0.293		10.7%	0.33%	33.1
k_{25}	0.251	0.246		7.8%	0.27%	30.1
k_3	0.396	0.416		7.8%	0.26%	28.8
k_4	3.017	2.786		8.2%	0.25%	35.1
k_5	3.294	3.483		15.3%	0.34%	42.0
k_6	2.248	2.074		32.2%	1.28%	27.2

TABLE VII. IDENTIFICATION RESULTS FOR THE COMPENSATOR ELASTOSTATIC PARAMETERS

Elastostatic parameters	Unit	Value	Confidence interval
k_c	[rad × μm/N]	0.144	±0.031
s_0	[mm]	458	±27
k_2^0	[rad × μm/N]	0.302	±0.004

TABLE VIII. MANIPULATOR ACCURACY IMPROVEMENT AFTER ELASTOSTATIC CALIBRATION BASED ON RESIDUAL ANALYSIS

Type of residuals		Before calibration	After calibration	Improvement factor
Coordinate based, [mm]	***max***	9.17	1.53	6.0
	RMS	2.99	0.46	6.5
Distance based, [mm]	***max***	9.26	1.54	6.0
	RMS	5.18	0.80	6.5

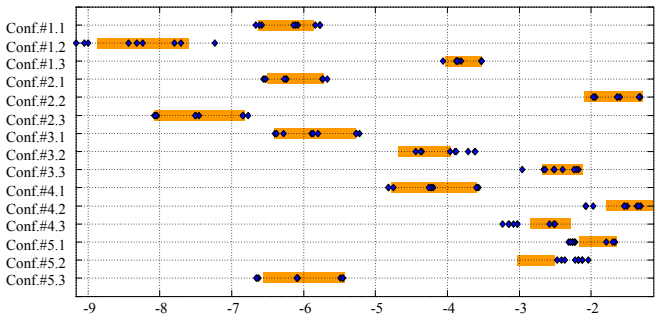

Figure 5. Distributions of the manipulator end-effector deflections along Z directions: ♦ - experimental data; - computated

To evaluate the calibration results, let us analyze the residuals computed from the identification equations for each coordinate separately. It is worth mentioning that the residuals after calibration along Z-direction are in a good agreement with those obtained in the geometric case. In contrast, in X and Y-direction the error deviations are higher because of the model limitation, which is not able to describe the deflections in these two directions without taking into account the elastostatic property of joint #1. Nevertheless, the elastostatic calibration ensures essential improvement of the robot accuracy. As follows from the results, the positioning errors evaluated using the model are in a good agreement with the ones obtained via residual analysis based on experimental data (Figure 5). In fact, the developed calibration technique is able to compensate in average 95% of the deflections in Z-direction. Hence, the obtained elastostatic model is able to provide quite reasonable estimates of the end-effector positioning errors for all manipulator configurations under the loading.

V. Experimental Validation

A. Validation methodology

To justify the obtained results, it is reasonable to evaluate them for additional configurations that were not employed in the calibration. In the frame of this idea, experimental data have been divided into two non-overlapping subsets:

- Calibration subset, which has been used for identification of the model parameters;
- Validation subset, which has been used for evaluation of the model accuracy after calibration.

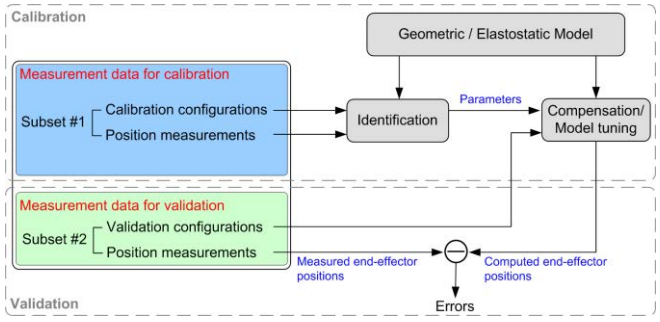

Figure 6. Validation scheme for the calibration results

Then, for each measurement from the validation subset, the difference between the measured end-effector position and the computed position (using the calibrated model) has been evaluated (Figure 6).

To demonstrate the advantages of the optimal pose selection technique (that has been used to generate measurement configurations both for geometric and elastostatic cases), the manipulator accuracy after calibration has been compared for two distinct plans of the calibration experiments. The first one has been obtained using the industry-oriented performance measure and numerical algorithms proposed in this work. In this case, the manipulator was presented as a quasi-serial chain (in order to take into account the gravity compensator impact), and the calibration data were obtained using the enhanced partial pose measurements. The second plan used measurement configurations that were selected semi-intuitively, in accordance with some kinematic performance measures [17]. Relevant manipulator model corresponds to the strict serial architecture, and the calibration data were obtained using conventional full-pose measurements.

Using these two sets of calibration data, the identification yielded two slightly different sets of manipulator parameters (Table IX). Then, the obtained parameters (both sets) may be used to compute the end-effector positions for the validation configurations. Comparing these results with the corresponding position measurements, it is possible to evaluate the "calibration quality" and relevant plans of the experiments (Figure 7).

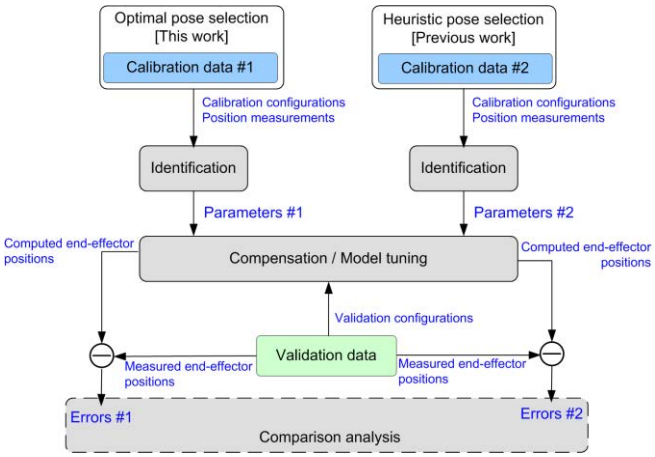

Figure 7. Validation scheme for the developed optimal pose selection technique

TABLE IX. Manipulator elastostatic parameters obtained using known and developed approaches, μrad/Nm

	k_1	k_2	k_3	k_4	k_5	k_6
[This work]	0.623	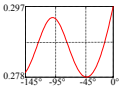	0.416	2.786	3.483	2.074
Previous work]	3.798	0.248	0.276	1.975	2.286	3.457

B. *Validation of the results for geometric calibration*

In order to validate the identification results for geometric parameters, the manipulator positioning accuracy after error compensation has been analyzed for each validation configuration separately. The geometric error distributions for these configurations are presented in Figure 8, corresponding histograms of errors in x, y and z direction are shown in Figure 9. As follows from detailed analysis, the errors have zero mean values and almost the same standard deviation σ, which is equal to 0.17 mm, 0.22 mm and 0.20 mm along X, Y, and Z directions, respectively. It should be noted that here the results tend to follow a normal distribution, however non-perfectly due to the insufficient statistical data (60 coordinates in each direction).

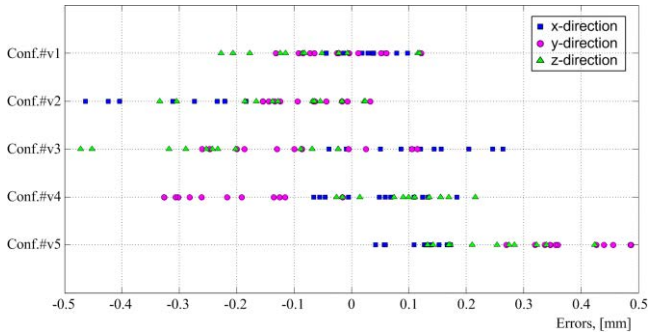

Figure 8. Geometric error distribution for validation configurations

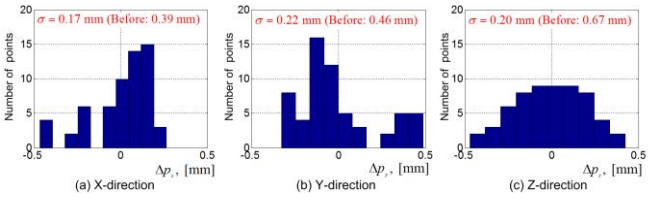

Figure 9. Histograms of error distribution along X, Y, and Z directions after geometric calibration (for validation configurations)

It is worth mentioning that the parameter σ estimated from the error analysis of the validation data is higher than the one computed on the identification step. This difference is caused by the limitation of the manipulator model used for calibration that does not take into account elastostatic properties. More detailed information is presented in Table X, which contains the positioning errors for each configuration and each end-effector reference point. It also provides the average positioning errors computed from the experimental data and using the covariance matrix. The results show that the model-based predicted errors are higher compared to the previous case (evaluated for calibration configurations) but they are in a good agreement with the ones obtained from experiments.

For comparison purposes, the manipulator accuracy improvement due to geometric errors compensation has been also studied based on the residual analysis before and after compensation. Relevant results are presented in Table XI, where the maximum and RMS values are provided. As follows from the obtained results, the geometric error compensation can ensure essential improvement of the robot accuracy. Here, the maximum errors have been reduced by a factor of 2.3 and 1.9 for these two criteria respectively, while the RMS errors have been decreased by a factor of 2.6.

TABLE X. POSITIONING ERRORS AFTER GEOMETRIC COMPENSATION FOR EACH VALIDATION CONFIGURATION (WITHOUT LOADING, MM)

Valid. config.	Coordinate-based residuals			Average positioning error	
	X	*Y*	*Z*	*Experiments*	*Model*
Conf.1	-0.04... 0.10	-0.13... 0.12	-0.23... 0.12	0.09	0.11
Conf.2	-0.46... -0.18	-0.15... 0.03	-0.33... 0.02	0.21	0.23
Conf.3	-0.04... 0.26	-0.26... 0.12	-0.47... -0.02	0.20	0.18
Conf.4	-0.07... 0.18	-0.33... -0.02	-0.03... 0.22	0.16	0.18
Conf.5	0.04... 0.17	0.27... 0.49	0.13... 0.42	0.28	0.12

TABLE XI. THE MANIPULATOR ACCURACY IMPROVEMENT AFTER GEOMETRIC ERROR COMPENSATION

Type of residuals		Before calibration	After calibration	Improvement factor
Coordinate based, [mm]	***max***	1.11	0.49	2.3
	RMS	0.52	0.20	2.6
Distance based, [mm]	***max***	1.28	0.66	1.9
	RMS	0.90	0.34	2.6

C. *Validation of the results for elastostatic calibration*

In order to evaluate the identification results for the elastostatic parameters, the manipulator positioning accuracy under loading has been analyzed separately for each validation configuration. For these configurations, the histograms of the elastostatic error distributions after compensation are presented in Figure 10. As follows from their analysis, the RMS values of these errors are equal to 0.21 mm, 0.44 mm and 0.21 mm along X, Y, and Z directions, respectively. It should be noted that here the results of positioning errors tend to follow the Maxwell-Boltzmann distribution with the overall standard deviation of 0.14 mm, however due to the insufficient statistical data, their shapes are slightly different from the theoretical one.

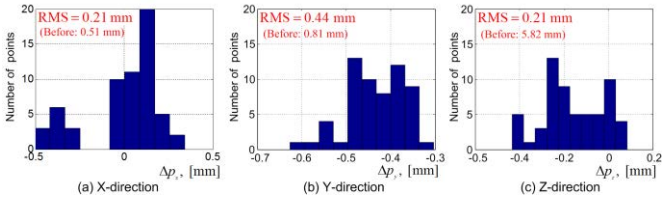

Figure 10. Histograms of error distribution along X-, Y-, and Z-directions after elastostatic calibration (for validation configurations, data subset #2)

It is worth mentioning that the manipulator positioning accuracy after elastostatic errors compensation along X- and Z-directions (with the RMS value equal to 0.21 mm) justifies the effectiveness of the proposed calibration technique (provided accurate manipulator parameter estimations).

While the accuracy along Y-direction is not perfectly improved because of the model limitation, which is not able to describe these deflections completely. Nevertheless, as it will be shown below, the elastostatic calibration ensures essential improvement of the robot accuracy. In more details, the positioning errors concerning each configuration and each reference point are provided in Table XII. Similar to the geometric case, the average positioning errors are computed from the experimental data and using the covariance matrix, corresponding results indicate good agreement between these two approaches.

For comparison purposes, the manipulator accuracy improvement due to elastostatic errors compensation has been studied based on the error analysis before and after compensation. Relevant results are presented in Table XIII. As follows from the obtained results, using the identified elastostatic parameters, it is possible to compensate essentially the deflections along Z-direction (96.4% in average). In general, the manipulator positioning accuracy has been improved by a factor of 11.1 compared to a non-compensated robot.

TABLE XII. POSITIONING ERRORS AFTER ELASTOSTATIC CALIBRATION FOR EACH VALIDATION CONFIGURATION (SUBSET #2, UNDER LOADING, MM)

Valid. config.	Coordinate-based residuals			Average positioning error	
	X	*Y*	*Z*	*Experiments*	*Model*
Conf.1	-0.46… -0.24	-0.49... -0.37	-0.15... 0.09	0.31	0.54
Conf.2	0.07... 0.39	-0.52... -0.30	-0.24... -0.09	0.32	0.52
Conf.3	-0.03... 0.21	-0.63... -0.40	-0.43... -0.23	0.36	0.26
Conf.4	0.03... 0.21	-0.42... -0.34	-0.29... -0.17	0.26	0.27
Conf.5	0.05... 0.22	-0.44... -0.34	-0.19... 0.03	0.25	0.22

TABLE XIII. THE MANIPULATOR ACCURACY IMPROVEMENT AFTER ELASTOSTATIC ERROR COMPENSATION

Crite-rion		Coordinate-based residual, [mm]				
		Before compen-sation	After compensation		Improvement factor	
			*[Previous work]**	*[This work]***	*[Previous work]**	*[This work]***
X	*max*	0.79	0.51	0.46	1.5	1.7
	RMS	0.51	0.23	0.21	2.1	2.4
Y	*max*	1.35	0.68	0.63	1.9	2.2
	RMS	0.81	0.44	0.44	1.8	1.8
Z	*max*	8.06	1.63	0.43	4.9	18.7
	RMS	5.82	1.17	0.21	5.0	28.0
		Distance-based residual, [mm]				
	max	8.28	1.77	0.78	4.6	10.4
	RMS	5.90	1.27	0.53	4.6	11.1

*Stiffness model does not take into account the gravity compensator impact
**Stiffness model takes into account the gravity compensator impact

VI. CONCLUSION

The paper is devoted to the experimental study. Particular attention has been paid to the positioning accuracy improvement of KUKA KR-270 industrial robot that includes the gravity compensator. For this robot positioning accuracy has been improved by the factors 6 and 10 for the unloaded and loaded manipulator respectively. The paper summarises experimental study on accuracy improvement in robotic-based manufacturing conducted in the frame of national research program associating academic and industrial partners.

ACKNOWLEDGMENT

The work presented in this paper was partially funded by the ANR (Project ANR-2010-SEGI-003-02-COROUSSO), France and FEDER ROBOTEX, France.

REFERENCES

[1] M. Vukobratović and D. Vujić, "Contribution to solving dynamic robot control in a machining process," Mechanism and Machine Theory, vol. 22, pp. 421-429, // 1987.
[2] H. W. Stone, Kinematic modeling, identification, and control of robotic manipulators vol. 29: Springer, 1987.
[3] J. M. Hollerbach, "A survey of kinematic calibration," in The robotics review 1, ed: MIT Press, 1989, pp. 207-242.
[4] B. W. Mooring, Z. S. Roth, and M. R. Driels, Fundamentals of manipulator calibration: Wiley New York, 1991.
[5] A. Elatta, L. P. Gen, F. L. Zhi, Y. Daoyuan, and L. Fei, "An overview of robot calibration," Information Technology Journal, vol. 3, pp. 74-78, 2004.
[6] A. Joubair, M. Slamani, and I. A. Bonev, "Kinematic calibration of a five-bar planar parallel robot using all working modes," Robotics and Computer-Integrated Manufacturing, vol. 29, pp. 15-25, 2013.
[7] G. Alici and B. Shirinzadeh, "Enhanced stiffness modeling, identification and characterization for robot manipulators," Robotics, IEEE Transactions on, vol. 21, pp. 554-564, 2005.
[8] A. Nubiola and I. A. Bonev, "Absolute calibration of an ABB IRB 1600 robot using a laser tracker," Robotics and Computer-Integrated Manufacturing, vol. 29, pp. 236-245, 2013.
[9] J. Hollerbach, W. Khalil, and M. Gautier, "Model Identification," in Springer Handbook of Robotics, B. Siciliano and O. Khatib, Eds., ed: Springer Berlin Heidelberg, 2008, pp. 321-344.
[10] A. Klimchik, Y. Wu, S. Caro, and A. Pashkevich, "Design of experiments for calibration of planar anthropomorphic manipulators," in Advanced Intelligent Mechatronics (AIM), 2011 IEEE/ASME International Conference on, 2011, pp. 576-581.
[11] J.-H. Borm and C.-H. Menq, "Determination of Optimal Measurement Configurations for Robot Calibration Based on Observability Measure," The International Journal of Robotics Research, vol. 10, pp. 51-63, 1991.
[12] W. Khalil, M. Gautier, and C. Enguehard, "Identifiable parameters and optimum configurations for robots calibration," Robotica, vol. 9, pp. 63-70, 1991.
[13] D. Daney, Y. Papegay, and B. Madeline, "Choosing measurement poses for robot calibration with the local convergence method and Tabu search," The International Journal of Robotics Research, vol. 24, pp. 501-518, 2005.
[14] A. Klimchik, Y. Wu, A. Pashkevich, S. Caro, and B. Furet, "Optimal Selection of Measurement Configurations for Stiffness Model Calibration of Anthropomorphic Manipulators," Applied Mechanics and Materials, vol. 162, pp. 161-170, 2012.
[15] A. Klimchik, Y. Wu, C. Dumas, S. Caro, B. Furet, and A. Pashkevich, "Identification of geometrical and elastostatic parameters of heavy industrial robots," in Robotics and Automation (ICRA), 2013 IEEE International Conference on, 2013, pp. 3707-3714.
[16] A. Klimchik, Y. Wu, S. Caro, B. Furet, and A. Pashkevich, "Advanced robot calibration using partial pose measurements," in Methods and Models in Automation and Robotics (MMAR), 2013 18th International Conference on, 2013, pp. 264-269.
[17] C. Dumas, "Développement de méthodes robotisées pour le parachèvement de pièces métalliques et composites," Université de Nantes, 2011.